Journal of The Electrochemical Society

Increased Moisture Uptake of NCM622 Cathodes after Calendering due to Particle Breakage

Journal of The Electrochemical Society, 2021 **168** 090539

Increased Moisture Uptake of NCM622 Cathodes after Calendering due to Particle Breakage

Fabienne Huttner,[1,2,z] Alexander Diener,[1,2] Thilo Heckmann,[3] Jochen C. Eser,[3] Tugay Abali,[1,2] Julian K. Mayer,[1,2] Philip Scharfer,[3] Wilhelm Schabel,[3] and Arno Kwade[1,2]

[1]*Institute for Particle Technology, Technische Universität Braunschweig, Germany*
[2]*Battery LabFactory Braunschweig, Technische Universität Braunschweig, Germany*
[3]*Karlsruhe Institute of Technology, Thin Film Technology, Germany*

As moisture presents a critical contamination in lithium-ion batteries (LIBs), electrodes and separators need to be post-dried before cell assembly. The moisture adsorption, desorption and re-adsorption of electrodes during processing is strongly dependent on their material system, manufacturing route and microstructure. The microstructure, in turn, is significantly defined by the coating density, which is adjusted by calendering. As a consequence, the calendering step is expected to directly influence the moisture sorption behavior of electrodes. This is why the influence of different coating densities and structural properties on the moisture content of NCM622 cathodes was investigated in this study. For increasing density, an increasing moisture content was detected by Karl Fischer Titration and sorption measurements. SEM and BET analyses showed an increasing amount of NCM622 particle breakage, accompanied by a rising surface area. Hence, the increased moisture uptake of cathodes with higher density is mainly caused by a higher surface area, which results from particle cracking and breakage during calendering. Electrochemical analysis showed that the increased active surface area of cathodes with higher densities leads to a good performance during formation and at low C-rates. However, the reduced porosity impairs the ionic conductivity and causes capacity loss at higher C-rates.
 [DOI: 10.1149/1945-7111/ac24bb]

Manuscript submitted August 3, 2021; revised manuscript received August 27, 2021. Published September 20, 2021.

Due to the paradigm shift in the global energy supply towards renewable energy, lithium-ion batteries (LIBs) play a key role in stationary energy storage systems and especially in electric vehicles (EVs), which require a low-cost and high-performance energy storage technology.[1,2] In fact, the growing success of EVs can be attributed to the progress made in electrochemical storage technologies and their manufacturing process over the past decades, increasing the specific energy of LIBs from approximately 90 Wh kg^{-1} cell to over 250 Wh kg^{-1} cell and simultaneously reducing its cost from over 1000 US$ kWh^{-1} to under 250 US$ kWh^{-1}.[2] Low-cobalt, Ni-rich layered $LiNi_{0.6}Co_{0.2}Mn_{0.2}O_2$ (NCM622) turned out to be a viable choice for cathode active material in LIBs, as it meets the requirements of high energy density and sufficient safety, and achieves good reversible capacities.[3–5] However, although the characteristics of LIBs and their components are well acknowledged today, the different steps in the process chain need to be continually developed or improved to meet the growing demands on performance and safety.[5–7] In particular, the impact of the different process steps on mechanical, physical, and electrochemical properties and the mutual interference need to be understood more deeply to be able to further improve LIBs. Another question which has to be addressed to improve performance and safety is the impact of contaminations. Here, moisture and, thus, water presents a quite critical contamination.[5,8,9] There are basically two ways water can come into the electrodes: Firstly, during the preparation of the electrode slurry, trough moisture uptake of the raw materials or by the solvent, either due to using water as solvent or by water uptake of the solvent. Especially after wet processing of electrodes with water as solvent, thousands of ppm can remain after the initial drying process. Secondly, electrodes can absorb the moisture from their surrounding atmosphere during further processing like calendering or slitting.[5] If the moisture is not sufficiently reduced before cell assembly, it can undergo unwanted side reactions with the conducting salt $LiPF_6$ during cycling, which is commonly used in organic electrolytes for LIBs.[5,8–10] These side reactions cause the formation of gaseous hydrogen fluoride (HF) and further acidic decay products. This poses a high safety risk as it can cause explosion due to increasing cell pressure.[5,8–10] Furthermore, the decay products can cause decomposition of the active materials, impede the formation of an effective solid electrolyte interface (SEI) or attack an already formed one.[5,9–13] In order to reduce the moisture in the cell below a critical level, electrodes and separators for LIBs need to be post-dried before cell assembly. However, the moisture adsorption, desorption and re-adsorption behavior of the electrodes is strongly dependent on the chosen material system, the manufacturing route as well as the microstructure of the electrodes.[5,8,14]

The microstructure, in turn, is significantly defined by the calendering step, which primarily aims at increasing the specific density and, by that, the volumetric energy density of the electrode coatings. It determines not only the final porosity of the electrode coating, and thereby the electric and ionic conductivity, but also mechanical strength, elasticity, adhesion and homogeneity of the coating.[6,15,16] At industrial scale, the compaction is realized by passing an electrode web through one or multiple pairs of rolls and controlling the intensity of the compaction either through varying the gap size or by setting the force between the rolls.[7,15,16] Increasing the densification rate usually reduces the electrical resistance and benefits the adhesive force at higher compaction rates. The increase of electric conductivity usually leads to a higher cycle stability and a higher C-rate performance of NCM cathodes.[15,17,18] However, a compaction exceeding a critical value can fracture the NCM particles, damage the current collector, and limit the ionic diffusion due to the decreased porosity, resulting in a reduced available capacity at high currents.[15] In addition, Appiah et al.[19] stated that NCM622 cathodes have a peak in performance while having a porosity of around 20% on low mass loadings (30 μm coating thickness) and around 30% on high mass loadings (70 μm coating thickness). Calculated on the basis of density values for NCM622,[19] carbon black[20] and the binder used, polyvinylidene fluoride (PVDF),[20] these coating thicknesses correspond to mass loadings of approximately 9.7 mg cm^{-2} and 19.8 mg cm^{-2}. According to Appiah et al.[19] the choice of the appropriate porosity for the respective mass loading ensures a high electrical conductivity while maintaining a fully developed pore network, which is needed for a sufficient ionic conductivity at high currents.

Although the calendering step has already been investigated by many researchers,[4,7,15–28] to our knowledge its influence on moisture uptake and release of the electrodes has not been investigated in detail until now. However, as calendering has a significant impact on

[z]E-mail: fabienne.huttner@tu-braunschweig.de

the microstructure of the electrodes, it can be assumed that it correspondingly influences the moisture sorption behavior of the electrodes during further processing and the moisture desorption during post-drying. Eser et al.[14] assumed that the sorption equilibrium of water in electrodes is dependent on the surface of the particles, on sorption in the binder and, to a certain degree, on capillary condensation within the pores and between the particles. As PVDF is strongly hydrophobic,[8,29] the water sorption in the binder is assumed to be very low in PVDF cathodes. According to Langklotz et al.[10] ,the moisture sorption behavior of NCM cathodes with PVDF binder is determined by the active surface of the electrode. Stich et al.[9] also stated that the specific surface area of the electrode materials has the highest impact on the moisture content of electrodes materials. In a previous study, it was shown that there is a hysteresis in the sorption behavior of NCM622 cathodes.[8] In literature, hysteresis behavior of porous materials is often traced back to the irreversibility of capillary condensation.[30–33] Hence, the proven hysteresis behavior of the cathodes could indicate the presence of capillary condensation within NCM622 cathodes. Consequently, the moisture sorption of NCM cathodes with PVDF can be assumed to be fundamentally determined by surface adsorption and, presumably to a smaller degree, by capillary condensation. In contrast, the substantially higher moisture uptake of graphite anodes with carboxymethyl cellulose (CMC)/styrene-butadiene rubber (SBR) binder in comparison to PVDF cathodes is mainly caused by the hygroscopic binder system.[5,8,14] Thus, the sorption behavior of graphite anodes is almost exclusively determined by moisture sorption in the hygroscopic binders, especially in CMC. In comparison, surface adsorption and capillary condensation play a subordinate role.[14]

As the calendering step crucially influences the porous structures and the particle surfaces in the coating, but does not change the chemical condition of the binder system, its impact is expected to be especially pronounced in LIB cathodes with PVDF binder. This is why the influence of different coating densities on moisture content and structural properties of NCM622 cathodes for LIBs is investigated in this study.

Experimental

Electrode composition and manufacturing.—For the cathode manufacturing, common materials were used. The recipe consisted of 95.5 wt% $LiNi_{0.6}Co_{0.2}Mn_{0.2}O_2$ (NCM622, BASF) as active-material, 1.5 wt% carbon black (C-Nergy Super C65, Imerys) and 0.75 wt% graphite (Timrex SFG6L, Imerys) as conductive agents as well as 2.25 wt% polyvinylidene fluoride binder (PVDF Solef 5130, Solvay). *N*-methl-2-pyrrolidon (NMP, electrochemical grade, BASF) served as solvent. The NCM622 cathodes were produced in one batch using a planetary mixer PMH10 (NETZSCH Feinmahltechnik GmbH, Germany) with the same settings as in a previous study.[5] As mixing tools, a high-speed stirrer with double butterfly setup, a cross-beam low-speed stirrer and a baffle rotating along the mixing vessel wall were installed.

Coating and drying were conducted in a pilot-scale continuous convective coating and drying machine LabCo with a comma bar (Kroenert GmbH & Co. KG, Germany). The cathode slurry was coated onto an aluminum current collector foil of 20 μm thickness (Hydro Aluminium GmbH, Germany) with a mass loading of 30 mg cm^{-2} and a coating width of 180 mm. The high mass loading was chosen to be able to identify a clear impact of the calendering step on the moisture content of the cathode and corresponds to an area capacity of 5.15 mAh cm^{-2}. The speed of the drying machine was adjusted to 2 m min^{-1} and the temperatures of the three drying segments with 2 m lengths each were set to 80 °C, 100 °C and 120 °C.

Calendering.—The cathodes with an initial density of 2.6 g cm^{-3} were continuously calendered to densities of 2.8, 3.0 and 3.2 g cm^{-3} using the lab scale two-roll compactor GKL 300 L (Saueressig GmbH & Co. KG, Germany) with roll diameters of 200 mm and roll widths of 300 mm. The roll gap was varied to reach the desired cathode densities while the calendaring speed was constant with 1 m min^{-1}. The differently compacted cathodes were rolled to coils of 15 m lengths each.

Post-drying procedure.—Post-drying of the coils was conducted in a vacuum oven VD 115 with a pump VAP 1 (final pressure 7 mbar, Binder GmbH & Co. KG, Germany) and a vacuum controller CVC3000 (Vacuubrand GmbH & Co. KG, Germany) which is installed in a dry room with a dew point of ∼−40 °C. The same post-drying procedure as in a previous study[8] was used. It consisted of a 2 h heating phase to 80 °C under atmospheric pressure and a 4.7 h post-drying phase at 80 °C with 14 Argon purging cycles between 10 and 30 mbar. The achievement of the target temperature of 80 °C inside the coils was validated with temperature measuring stripes (Reatec-AG©, Switzerland). For further details, see Huttner et al.[8]

Determination of water content via Karl Fischer Titration.—The moisture content of the cathodes was measured via coulometric Karl Fischer Titration (KFT, Aqua 40.00 with headspace module, ECH Elektrochemie Halle GmbH, Germany). Therefore, the vials with the cathode samples were placed in the KFT oven, which was pre-heated to 120 °C. The samples taken before post-drying were measured for a duration of 10 min. After post-drying, the duration was raised to 20 min as the low moisture contents of the cathodes were already close to the lower limit of the resolution area of the KFT and differences of few ppms have a great impact on the result and its reproducibility. The measuring temperature was determined beforehand with the help of temperature ramps and comparison of moisture measurements at different temperatures and finally set as low as possible to reproduce practical post-drying conditions and to prevent side reactions or the removal of chemically bound water.[5,8,9,34] For each analysis, a threefold measurement was conducted and averaged (for the value of the cathode with a density of 3.0 g cm^{-3} after post-drying, only one measurement was taken as the other two were measured incorrectly). As the current collector foils only adsorb very small amounts of moisture, the measured moisture was considered to come solely from the coating. Therefore, the moisture contents in ppm were calculated only in relation to the weight of the coating. Further details regarding the measuring principle can be found in Huttner et al.[5]

Measurements of sorption equilibria.—A magnetic suspension balance (MSB) enclosed in a conditioned measurement cell determines sorption equilibria with a resolution of up to 1 ppm. The continuous flow of a controlled mixture of a solvent saturated and a dry (dew point temperature < -65 °C) nitrogen flow through the measurement cell conditions this cell. A chilled-mirror hygrometer precisely monitors the dew point temperature of the nitrogen flow entering the measurement cell. This set-up enables an accurate adjustment of the solvent activity in the measurement cell between 0 and 0.3 which is the relevant range for the considered conditions of the process chain. This experimental set-up has been established and thoroughly described in previous studies.[14,35,36] A common equation to describe the sorption equilibrium at low solvent activity of an adsorption onto a solid surface is the Brunauer–Emmett–Teller (BET) isotherm.[37] In contrast to Langmuir's theory[38] of gas adsorption the BET isotherm accounts for multilayer adsorption and is given as follows:[37]

$$X = \frac{X_m \cdot k_{BET} \cdot a}{(1 - a) \cdot (1 + (k_{BET} - 1) \cdot a)} \quad [1]$$

The parameter a is the activity of the adsorbate and X the respective loading. The fit parameters k_{BET} and the monolayer loading X_m must be fitted to the sorption data to obtain the BET isotherm. The monolayer loading holds information about the surface area of a

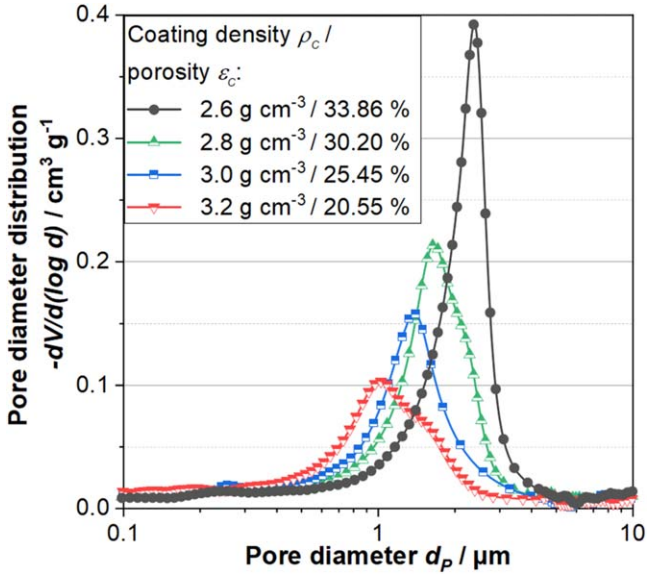

Figure 1. Pore size distribution of the produced cathodes (derived from one measurement each) with indication of density and porosity (averaged from two measurements).

sorbate:

$$A_{BET} = X_m \cdot A_i \cdot \frac{N_A}{\tilde{M}_i} \quad [2]$$

The surface area of a sorbate can be derived with the Avogadro constant N_A, the molar mass of the adsorptive $\tilde{M}_i$ and the surface area, that an adsorbed sorbate molecule occupies (A_i).[37] These areas are 12.5 Å^2 for water and 16.2 Å^2 for nitrogen at 25 °C.[37]

Electrode characterization.—The adhesion strength and the electric resistance were determined with a uniaxial material testing machine (Z020, Zwick GmbH & Co. KG, Germany). The adhesion strength measurements were conducted according to Haselrieder et al.,[39] the measurements regarding the electrical resistance according to Westphal et al.[40] For each measurement, 8-10 samples were measured and averaged. The porosity and the pore size distribution were measured via mercury intrusion (PoreMaster 60, Quantachrome Instruments, USA). Further information is given by Froboese et al.[41] In addition, the specific surface area of the uncompacted and compacted electrodes was measured via gas adsorption experiments and determined by the BET method. Therefore, the electrode samples were pretreated to reduce the moisture at 100 °C in a Nitrogen/Helium gasflow for 4 h and then measured using Nitrogen as analysis gas in the device Nova 200 e (Quantachrome GmbH & Co. KG, Germany). The BET surface area was calculated with the software NovaWin (version 11.03.).

Scanning electron microscopy.—The optical analysis of the cathodes with different densities was conducted by a scanning electron microscope (SEM, Phenom XL, Thermo Fisher Scientific Inc., USA). This SEM attains a resolution of <14 nm with a primary beam voltage of 30 kV and a pressure of 0.1 Pa in the sample chamber. The SEM-images were taken at 10 kV and 5000-times magnification.

Cell assembly and analysis.—After post-drying, the samples were welded airtight and transferred into an Argon glovebox (Glovebox Systemtechnik GmbH, Germany). There, the bags were opened under Argon and the cathode die-cuts with 14 mm diameter were assembled to coin half cells of the type CR2032 using a 500 µm lithium metal foil as counter electrode. Furthermore, a porous glass fiber separator (Whatman GF/D, cytiva, USA) and the electrolyte LP57 (Gotion Inc., USA) with 1 mol $LiPF_6$ and 2 vol.% vinylene carbonate (VC) were applied. The cells were then tested in a temperature-controlled battery testing machine (Series 4000, Maccor Inc., USA) at 21 °C. After a rest step of 24 h, three cycles of formation with 0.1 C charge and discharge followed by a first C-rate test (0.2/0.2, 0.2/0.5, 0.2/1.0, 0.2/2.0, 0.2/3.0 C charge/discharge; three cycles each) with theoretical capacity were conducted. After that, two cycles of recovery (0.1/0.1 C charge/discharge) and 10 cycles of cycling (1.0/1.0 C charge/discharge) followed. Then, four cycles of recovery (0.1/0.1 C charge/discharge) were conducted, the first two cycles with theoretical capacity, the last two cycles with the practical capacity, which had been retrieved after the formation in cycle. After that, the C-rate test and the cycling were repeated, this time with the practical capacity. At the end, four cycles of recovery (0.1/0.1 C charge/discharge) were conducted again, the first two cycles with practical capacity and the last two cycles with theoretical capacity. The upper and lower cut-off voltages were set to 4.2/3.0 V. For the analysis of the electrochemical performance, five cells were built and averaged for each density. As one cell of the cathode with density 2.8 g cm^{-3} stopped after cycle 37 due to technical reasons, only four cells were averaged from cycle 38 to 65 for this density.

Results and Discussion

The mechanical, physical, and electrochemical properties of LIBs are determined by numerous mutually influencing parameters. The calendering step and the resulting density of the electrodes have a significant influence on the microstructure of the electrodes. This is why they are expected to have a crucial impact not only on physical and electrochemical properties, but also on moisture sorption behavior, especially with regard to cathodes. In this study, the influence of different coating densities on moisture content and structural properties of LIB cathodes was addressed. To this end, a NCM622 cathode with PVDF binder, a mass loading of 30 mg cm^{-2} and an initial density of 2.6 g cm^{-3} was compacted to three different densities (low density = 2.8, medium density = 3.0 and high density = 3.2 g cm^{-3}), post-dried and assembled to half coin cells. The different states of the cathodes with distinct densities within the process chain were accompanied by measurements of the moisture, cohesion strength and electrical resistance and compared to the non-calendered state (2.6 g cm^{-3}). Furthermore, analyses on pore size distribution, sorption behavior and BET surface area were carried out and SEM-images were taken. The electrochemical performance was finally analyzed in half coin cells with C-rate tests and cycling.

Pore size distribution.—In Fig. 1, the pore size distribution and the porosity of the cathodes with different densities are displayed, both measured by mercury intrusion. The porosity is reduced with increasing density and the pore size distribution curve is compressed and shifted towards smaller pore diameters, which means that the coating contains smaller pores with rising densities. Due to the logarithmic scale, the impression arises that the peaks broaden with rising density. However, when comparing the absolute values, it can be observed that the peaks get narrower with increasing density. This indicates that at higher densities the coatings are not only less porous, but also more homogenous, as the pore size distribution lies within a smaller range.

Moisture content.—In Fig. 2, the moisture content of the cathodes along the process chain from the coated and dried state up to cell assembly is presented. In general, the moisture content of the cathode is comparatively low. This can be explained by the usage of the hydrophobic binder PVDF with NMP as solvent as well as the low specific surface area of NCM cathodes.[3,5,9,29] After coating and drying and before calendering, the cathode contains only 261 ppm moisture. Just by transporting the cathode into a dry room and exposing it to dry air with a dew point around −40 °C for 2.5 h

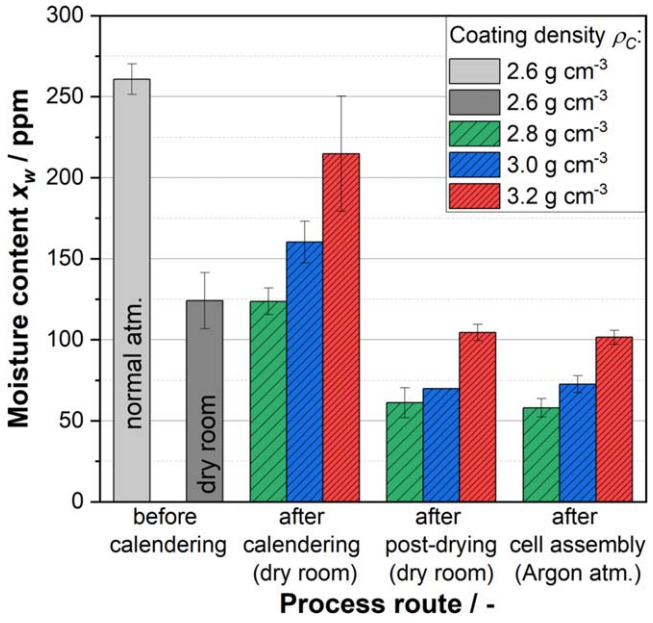

Figure 2. Moisture content of the cathodes at different process steps, measured via coulometric KFT (calculated without current collector).

before compaction, the moisture is reduced by 53% to 124 ppm, which indicates that the majority of the moisture in the cathode is bound weakly and can be easily removed.[5] After calendering the cathodes to different densities of 2.8, 3.0 and 3.2 g cm^{-3}, an increasing moisture uptake can be detected with increasing density. While the moisture content does not change after slight compression to 2.8 g cm^{-3}, after compression to 3.0 g cm^{-3} it increases by 29% to 160 ppm and after compression to 3.2 g cm^{-3} even by 73% to 215 ppm. Post-drying significantly reduced the moisture of all three cathodes by an average of 53%, although, the same course trend be seen with the lowest moisture detected at 2.8 g cm^{-3} and the highest at 3.2 g cm^{-3} density. Here, it must be noted that remoistening occurs immediately after post-drying as the electrodes are punched and packaged in the dry room, afterwards. Thus, as the electrode with the highest density adsorbed the highest moisture content before post-drying due to structural characteristics, it also adsorbs the highest moisture content after post-drying during remoistening. However, due to their hysteresis behavior, the cathodes remoisten to a lower moisture value than they contained before post-drying.[8,35] After cell assembly under Argon atmosphere, the moisture content of the cathodes stays at the same level. This indicates that the residual moisture after post-drying and further processing in the dry room cannot be further reduced by merely exposing the cathodes to Argon atmosphere.

SEM analysis.—As mentioned above, the moisture sorption of NCM cathodes with PVDF is assumed to be almost exclusively determined by surface adsorption and, to a smaller degree, by capillary condensation. Hence, the explanation for the increasing moisture uptake of cathodes with increasing density after calendering can most likely be traced back to different surface areas after calendering. To examine this assumption, further characterization methods were conducted. In Fig. 3, SEM images of the cathodes with the three different densities are compared to the non-calendered state. It can be seen that already after a weak compression to a density of 2.8 g cm^{-3}, some secondary active material particles, especially the coarser ones, show cracks of different sizes (cf Fig. 3b). With increasing density, this phenomenon is becoming more pronounced: more cracks can be detected, and some particles are even broken into many fragments (cf Fig. 3c). At a density of 3.2 g cm^{-3}, many particles show cracks and some particles are broken into fragments and even into primary particles (cf Fig. 3d). This type of particle breakage due to compression has already been described in literature.[15,22,25,26,42] Furthermore, Oswald et al.[22] observed that the particle breakage in NCM622 cathodes caused by compression led to a higher specific surface area, whereby the area increased with increasing compression. Thus, it can be assumed that the increasing moisture uptake with increasing density is mainly caused by the presence of more particle cracks and breakages. These cracks and breakages cause a larger surface area of the cathodes and thereby enable a higher moisture adsorption after compression.

Sorption measurements and BET analysis.—To prove this theory, sorption measurements were carried out for the non-calendered (2.6 g cm^{-3}) and the high density cathode (3.2 g cm^{-3}, cf. Fig. 4). The y-axis displays the water content x_w of the cathode in parts per million. The x-axis plots the water activity a_w of the gas phase. Grey markers show the isotherm of the non-calendered cathode, the sorption is marked as solid points and the desorption as hollow points. Similarly, the calendered cathode is marked red. Both isotherms propagate in similar manner during sorption and desorption. This similarity indicates equal sorption mechanisms for both the calendered and non-calendered cathode. The sorption isotherms separate at low water activities and ascend up to the point where the desorption begins. The desorption isotherms have a similar shape and show an offset towards their respective sorption isotherm. This hysteresis behavior of NCM622 cathodes, as well as of graphite anodes, has already been observed in previous studies.[8,35] As expected, the calendered cathode adsorbs more water compared to the non-calendered cathode. The BET isotherms were obtained by fitting Eq. 1 to the data points. The results are plotted as red and grey lines for highest density and non-calendered, respectively.

Furthermore, the BET surface areas of the high density cathode and the non-calendered cathode were calculated based on the fit parameters (cf Eq. 2) gained by the water sorption measurements, and compared to the BET surface areas determined by N2 adsorption (cf Table I). Both the sorption equilibria and the nitrogen adsorption to the cathodes confirm the findings of the SEM evaluation of the different calendering levels. The surface areas increase, supporting the hypothesis that calendering increases the moisture uptake in cathodes primarily due to a larger surface area, caused by particle breakage during compression. In Fig. 5, the moisture content of the cathodes after calendering to different densities is displayed as a function of their BET surface area. As there is a linear dependency between both parameters, it can be concluded that the rise in moisture uptake with increasing density is to a first approximation entirely caused by moisture uptake of the enlarged surface area.

A further reason for the increasing moisture uptake with rising density could be a pronounced capillary condensation in the cathodes with higher density due to the reduction of the pore diameters. As the pore diameters also decrease with increasing density and, thus, with

Table I. BET surface areas of cathodes with different coating densities determined by N_2 and H_2O adsorption measurements.

Coating density ρ_c/g cm^{-3}	N_2 adsorption/m^2 g^{-1}	H_2O adsorption/m^2 g^{-1}
Non-cal./2.6	0.577	0.577
3.0	0.684	—
3.2	0.882	0.912

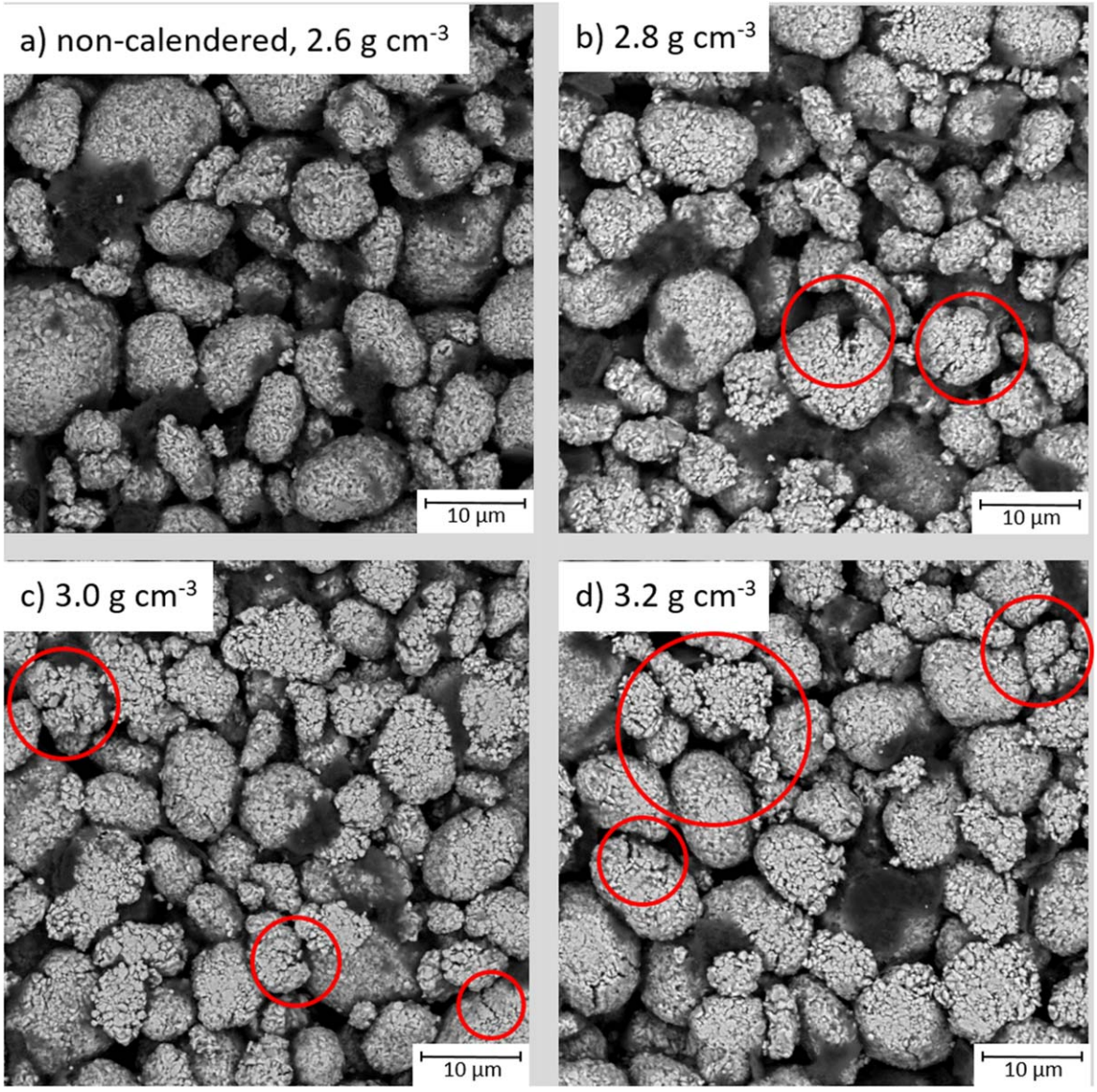

Figure 3. SEM surface images of the cathodes with different densities with markers of cracks in active material particles, 5000× magnification.

increasing BET surface, the effect of increased capillary condensation could still occur in parallel. Smaller pore diameters lead to an increased capillary pressure according to the Kelvin equation:[31,32,43,44]

$$\ln \frac{P}{P_0} = \frac{2\sigma V_m}{r_p RT} \quad [3]$$

In this equation, p represents the vapor pressure in the capillary, p_0 the saturation vapor pressure, σ is the surface tension of the liquid and V_m the molar volume. The (negative) pore radius is represented by r_p, the universal gas constant by R and the temperature by T. For a given water vapor pressure in the gas phase (given relative humidity), according to Eq. 3, a reduction of the pore diameters within the microstructure of the cathode due to calendering could contribute to the experimentally observed increase of moisture uptake by enhanced capillary condensation.[33,45,46] However, a definite distinction between the two mechanisms surface adsorption and capillary condensation requires further experimental work and will be the subject of future research.

Figure 6 shows a schematic representation of the moisture sorption at particle surfaces for the non-calendered and the high density cathode. Due to cracked or broken particles, there is a larger surface area at which moisture can be adsorbed after calendering. In addition, capillary condensation within the inner porosity of the secondary NCM particles and between the particles is featured.

Adhesion strength and electrical resistance.—To further investigate the influence of the different densities on the structure and, hence, properties of the cathodes, the adhesion strength and the electrical resistance of the cathodes were measured at different states of the process chain (Fig. 7). Note that a direct influence of the moisture content cannot be investigated precisely enough by these measurements as remoistening occurs during preparation and operation. However, conclusions concerning the influence of the post-drying step on the microstructure in general can be drawn.

The adhesion strength of NCM622 cathodes is generally determined by the mechanical strength of the PVDF binder matrix, which embeds the particles in the coating and builds contact points between particles and substrate.[39] The adhesion strength of PVDF results mainly from mechanical interlocking mechanisms and interfacial forces. The latter are only induced by weak van der Waals forces, and not by stronger reactive functional groups building polar intermolecular forces and bonds.[47] Hence, in contrast to the mechanical interlocking mechanisms, the interfacial forces of PVDF are hardly

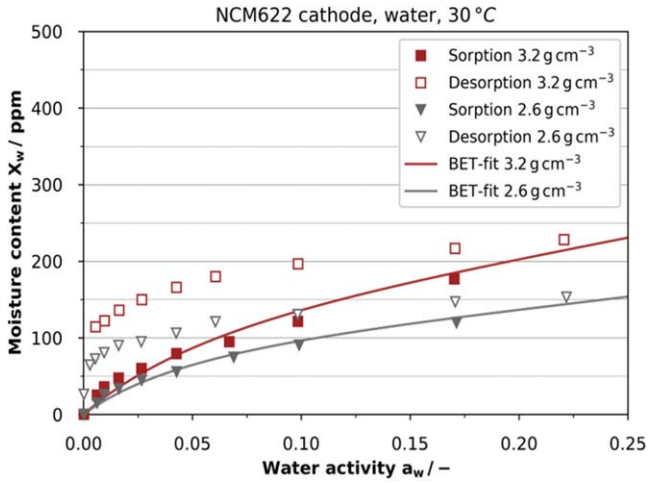

Figure 4. Comparison of the sorption equilibria of the non-calendered (2.6 g cm^{-3}) and the highest density (3.2 g cm^{-3}) cathode. A BET fit determined by the water sorption measurements describes the sorption isotherms and yields the parameters for the surface area determination.

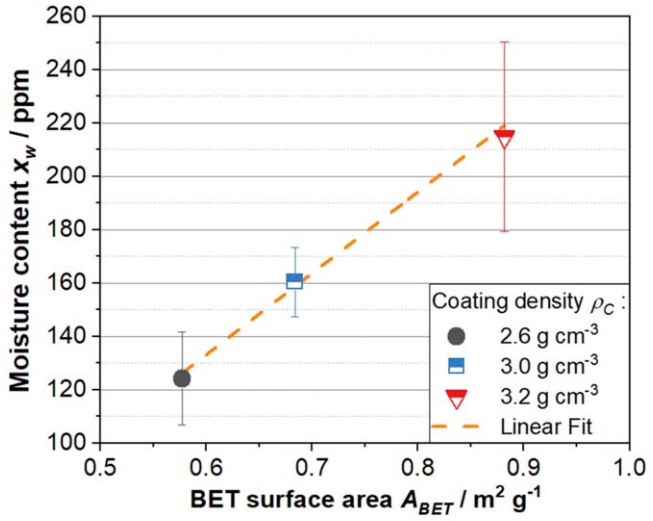

Figure 5. Moisture content of the cathodes after calendaring to different densities as a function of their BET surface area (determined by N_2 adsorption).

able to maintain the electrode's integrity during strain caused by further processing like calendering or during operation. Regarding the adhesion strength for different densities (Fig. 7, left), it can be detected that the adhesion strength first decreases with increasing compaction from 2.8 g cm^{-3} to 3.0 g cm^{-3}, before it increases again with further compaction from 3.0 g cm^{-3} to 3.2 g cm^{-3}. This behavior is well known in literature:[20] The first decrease of the adhesion strength can be addressed to different deformation behavior of the coating and the aluminum substrate leading to a shear stress, which damages the contact interface between the substrate and the coating. Further increase of the line load results in an increase of the adhesion strength due to a mechanical interlocking between the active material particles and the aluminum substrate.[20,23,27] For all densities and different states within the process route, cohesion failure can be observed by optical analysis. Hence, the interlocking between the coating and the aluminum substrate was higher than within the coating. Although the standard deviation of the values after post-drying is relatively high, a trend towards a rising adhesion strength after post-drying can be seen. Firstly, this proves that the chosen post-drying procedure is gentle enough to maintain the sensitive binder/carbon black (CB) network of the cathodes. Secondly, this could indicate that the higher temperatures during post-drying are able to rebuild contact points between coating and current collector and to reduce compression-induced defects in the electrode. These defects are often caused by plastic deformation at the interface between coating and current collector.[25] It may be, that post-drying leads to thermally activated creeping of the PVDF binder and thereby to a re-arrangement of contact points to a certain level.[5] Thirdly, the moisture reduction could also lead to better connection between substrate and coating. Bowden et al.[48] reported a decrease of friction between two surfaces after the admission of small amounts of water vapor. However, as the measurements cannot be conducted without remoistening of the samples, a direct influence of the moisture is difficult to identify.

By calendering, the porosity is reduced and the particles are arranged closer to each other. The contact points between the conductive agents are raised and the electric pathways are shortened, which improves the conductivity of the binder/particle network.[15,20,21,23,27,28,49] This leads to a reduction of the electrical resistance with increasing electrode density (Fig. 7, right). Post-drying leads to a small decrease of the electrical resistance for the cathode with the lowest density, to no changes for medium density and to a small increase for the cathode with the highest density. Thus, the influence of the post-drying step seems to be dependent on the porosity and the pore size distribution of the cathodes. A possible explanation could be that during post-drying, creeping of the thermoplastic binder PVDF is thermally activated.[5] In the cathode with higher density and hence lower porosity and smaller pores, the binder creeping may have led to local insulation in the smaller pores. However, this phenomenon should be addressed in further studies. Altogether, the results show that the sensitive binder/CB network is not seriously damaged by the chosen post-drying procedure as the changes in the electric resistance are very low.

Electrochemical performance.—In Fig. 8, the specific discharge capacities of half coin cells made from the differently compressed cathodes with an area capacity of 5.15 mAh cm^{-2} are displayed. For each density, five cells were built and averaged. As one cell of the cathode with density 2.8 g cm^{-3} stopped after cycle 37 due to technical reasons, only four cells were averaged from cycle 38 to 65 for this density.

In this study, very thick cathodes with a mass loading of 30 mg cm^{-2} and a thickness of 137 μm (including current collector) before calendering were investigated. This enables to identify the impact of different densities on the moisture contents of the cathodes. However, it is well known in literature that thick electrodes suffer from both low C-rate capability and cycle stability.[19,24,27,50,51] This phenomenon can be observed in the current study as well: During formation and at low C-rates, the cathodes show adequate discharge capacities. At higher C-rates, only lower discharge capacities are reached in general (cf Fig. 8). One reason for this effect are longer electric pathways within thick electrodes. Being accompanied by a higher amount of contact resistance points, they result in an increased electronic resistance of the coating.[27] In addition, thick electrodes suffer from deteriorated Li-ion diffusivity in the electrolyte.[50]

Comparing the different densities, during formation and at very low C-rates up to 0.5 C, the best performance is achieved by the cathode with the highest coating density (3.2 g cm^{-3}). However, at higher C-rates (1–3 C), this cathode performs significantly worse than those with lower densities. The cathodes with densities of 2.8 g cm^{-3} and 3.0 g cm^{-3} perform very similar and their standard deviations overlap each other. However, again the trend can be seen that the cathode with a higher density (3.0 g cm^{-3}) performs better at lower C-rates up to 0.5 C, whereas the cathode with lower density (2.8 g cm^{-3}) achieves higher discharge capacities at higher C-rates from 1−3 C.

The better performance of the higher density cathodes at low C-rates is in accordance with Oswald et al.[22] , who detected an increasing electrode capacity with rising compression and explained this by the increased electrochemically active surface area. Other researchers investigated crack formation in secondary NCM

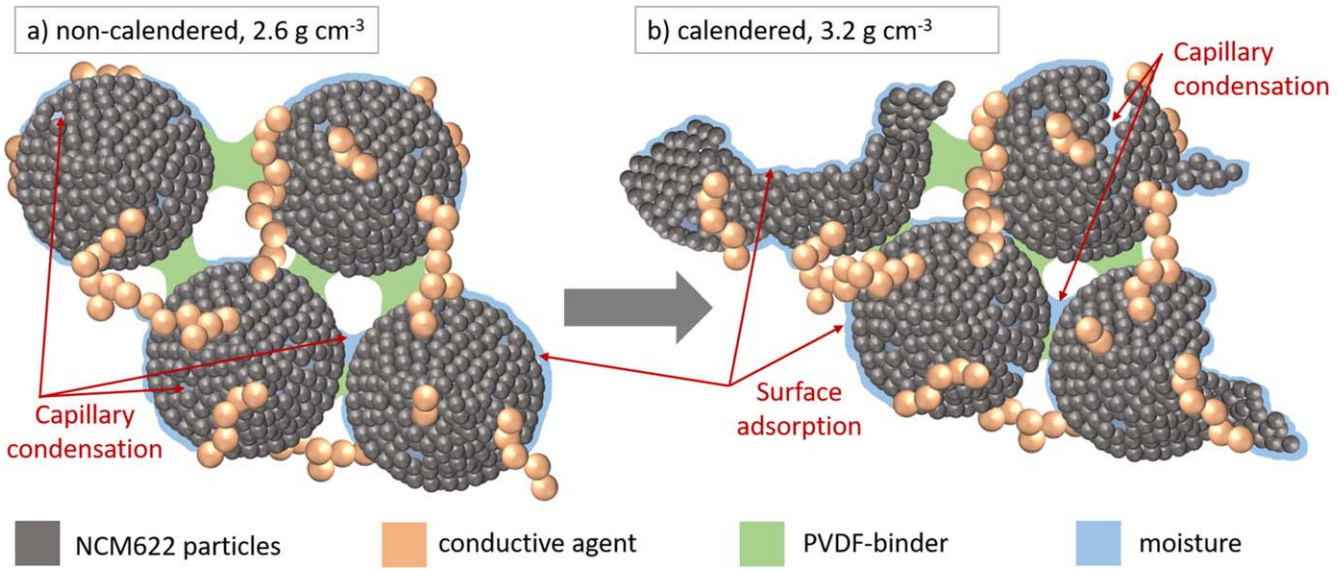

Figure 6. Schematic representation of moisture sorption at particle surfaces in the cathode coating in (a) the non-calendered state and (b) after compressing to 3.2 g cm^{-3}.

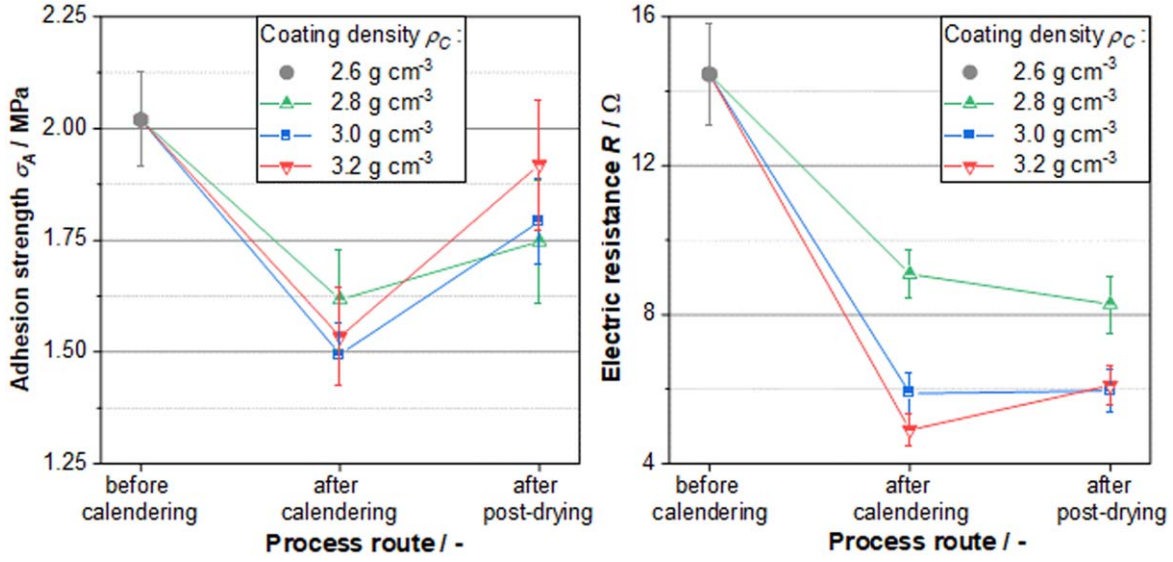

Figure 7. Adhesion strength and electrical resistance of the cathodes with different densities at different states in the process chain.

particles during the first charge and also detected an improved electrochemical performance due to increased electrochemically active surface areas and the associated reduced effective particle size.[52,53] Cracking was found to improve the liquid electrolyte infiltration in the active material particles and thereby lithium chemical diffusion, as well as charge transfer kinetics. Another reason for the good results of the higher density cathodes at low C-rates is the reduced electric resistance due to more conductive agent connections and shortened electric pathways.[23] Heubner et al.[50] stated that porosity reduction leads to an increase of specific ohmic and charge transfer resistance and a reduction of the Li-ion diffusivity, but also to a reduction of the contact resistance, which enhances the electric conductivity.

At low C-rates, the electrochemical performance is dependent on the specific ohmic, charge transfer, and contact resistance of the electrodes.[50] The ionic conductivity of the coating is not decisive for the electrochemical performance, as there is enough time for ion diffusion. In contrast, the electrochemical performance at high C-rates is defined by Li-ion diffusion in the electrolyte.[50] This explains the inversion of the electrochemical behavior of the cathodes at higher C-rates from 1 to 3 C. As high densities, or low porosities, cause Li-ion transport limitations, the performance at higher C-rates deteriorates with increasing compression.[27,50] The ion conductivity $k_{ion,analytical}$ is directly dependent on the porosity ε and the tortuosity τ of the coating and rises with increasing porosity and decreasing tortuosity:[49,54]

$$k_{ion,analytical} = k_{ion}^{bulk} \frac{\varepsilon}{\tau} \quad [4]$$

In this equation, k_{ion}^{bulk} represents the bulk ionic conductivity of the electrolyte. The tortuosity, in turn, takes in to account the windings or curves of the pores and can be described for example by the *Bruggemann* correlation:[41,49]

$$\tau = \frac{1}{\varepsilon^{0.5}} \quad [5]$$

According to the Bruggemann correlation, the tortuosity of the coating rises exponentially with decreasing porosity, lowering the Li-ion conductivity of the coating, and leading to capacity loss at

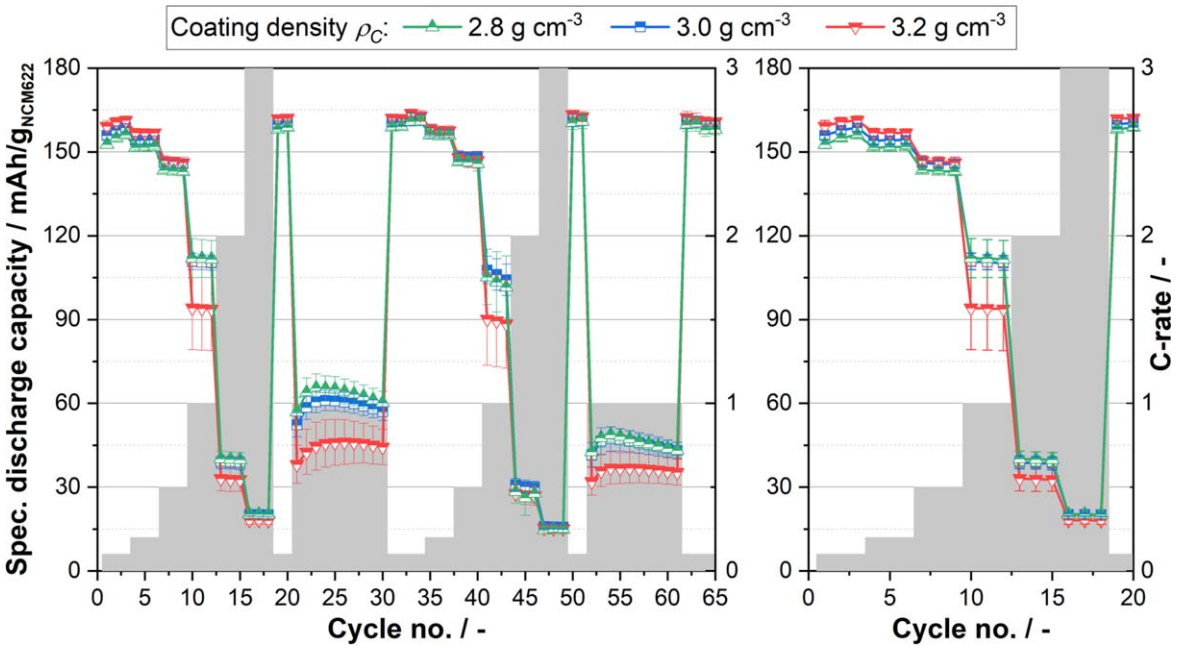

Figure 8. Specific discharge capacities of half coin cells made from the cathodes with different densities with indication of the respective C-rate. Left: presentation of 65 cycles containing 2 C-rate tests and 2 cycling phases. Right: Detailed presentation of the first 20 cycles.

higher C-rates. Furthermore, estimations of the energy density resulting for the cathodes in a typical pouch type lithium-ion battery cell show that at low C-rates the highest electrode density delivers the highest energy density, whereas at higher C-rates (1 C and higher) all three densities obtain similar energy density values.

Altogether, the higher electric conductivity of the high density cathode resulted in higher discharge capacities during formation and at low C-rates, compared to the lower density cathodes. In contrast, at higher C-rates (1–3 C), the lower ionic conductivity of the high density cathode affected the electrochemical performance. The corresponding ionic transport limitations led to lower discharge capacities, as there was not enough time for sufficient ion diffusion. Hence, the ionic transport limitations of the high density cathode negatively overlapped its better electric conductivity at C-rates of 1 C and higher. Here, due to their better ionic conductivity, the cathodes with lower densities performed better despite their lower electric conductivity.[50,55]

In general, during the second C-rate test and the second cycling phase, capacity fading can be observed at higher C-rates from 1−3 C, being a bit more pronounced for the lower density cathodes. According to Vetter et al.,[11] ageing of the cathode can be caused by structural changes during cycling, modifications of the surface film or chemical decomposition or dissolution reactions. In this study, capacity fading occurs only at higher C-rates, where the Li-ion diffusivity is the limiting process.[50] This indicates that the Li-ion diffusivity has been deteriorated, for example by the loss of Li-ions due to their consumption during chemical reactions or by the reduction of Li-ion mobility due to structural changes. However, ageing mechanisms were not the aim of this study and were therefore not analyzed in more detail.

The influence of the different moisture uptake levels on cell performance is difficult to investigate, as the discrepancies are caused by massive structural changes due to different compression. The impact of these structural changes is significantly higher than the different moisture contents in the cells, as the cells with highest moisture content performed best at low C-rates. In addition, residual moisture is especially problematic on the anodes' and separators' side as it impairs the formation of a well-functioning solid electrolyte interface (SEI), which protects the anode from degradation by the electrolyte.[5,8] However, if more moisture sensitive materials as NCM811 were used, the different moisture uptake might show more significant effects.

Conclusions

In this study, the influence of the calendering step and resulting differing densities on moisture adsorption and desorption of NCM622 cathodes was investigated. Therefore, a cathode with 30 mg cm^{-2} mass loading was compressed to three different densities (2.8, 3.0 and 3.2 g cm^{-3}), post-dried in a vacuum oven and assembled to half coin cells. The whole process route from the non-calendered state up to cell assembly was accompanied by moisture measurements and further analytics. It was observed that the moisture content of the cathodes increased with rising density after calendering. SEM images showed the well-known secondary NCM622 particle breakage after calendering,[15,22,25,26] which became even more pronounced with increasing density. Sorption measurements for the non-calendered (2.6 g cm^{-3}) and the high density (3.2 g cm^{-3}) cathode proved an increased moisture uptake of the high density cathode. In addition, the BET surface areas were determined and confirmed observations made in literature, which stated that the BET surface area of the cathodes increases with increasing density due to more pronounced particle breakage.[22] The moisture content showed a linear dependency on the BET surface area of the electrodes with different densities. Hence, the increased moisture uptake after calendering with increasing density was proven to be mainly caused by a higher surface area due to particle cracking and breakage.

Further analytics showed that the chosen post-drying procedure was gentle enough to maintain the sensitive binder/carbon black network of the cathodes. Regarding the cohesion strength, post-drying lead to an increase of the values. A possible explanation for this was given by a thermally activated recreation of the contact between coating and current collector, which was damaged during calendering before.[5,20,23,27] In addition, the reduction of moisture could have led to a better connection between substrate and coating.[48] The measurements of the electrical resistance displayed that the influence of the post-drying procedure depends on the density, as the electrical resistance decreased after post-drying for the low density cathode, stayed the same for the medium density cathode and increased for the high density cathode. As a possible

explanation, thermally activated creeping of the PVDF binder, which led to local insulations within smaller pores, was stated.[5]

During electrochemical tests, it was observed that the higher electrochemically active surface area of the highest density cathode in combination with more interconnected conductive agent particles and shortened electric pathways led to the best performance during formation and at low C-rates, compared to the other cathodes.[22,52,53] However, at higher C-rates, the reduced porosity and increased tortuosity impaired the ionic conductivity, which caused capacity loss.[16,27] In contrast, the cathodes with lower density performed better at higher C-rates and during cycling, which proved that a higher electrode porosity or a lower density is more important for a good C-rate capability than a higher electric conductivity of the coating due to higher densities.[24]

No measureable influence of the different moisture uptake of the cathodes on cell performance could be detected in this study, as the differences were caused by massive structural changes due to different compression. The influence of these structural changes was significantly higher than the different moisture contents in the cells. However, the influence of different amounts of moisture might have a more significant effect if moisture sensitive cathode materials with higher Nickel content were investigated.

Acknowledgments

The authors gratefully thank the German Federal Ministry of Education and Research (BMBF) for the financial support (Epic -03XP0295B and MiKal -03XP0240A) within the ProZell competency cluster. The authors also thank Arne Lüddecke, Tanja Boll, Rainer Severin, Jan-Michael Kröhnke, Alexander Neuberger, Axel Rosenkranz, Kerstin Krüger and Stoyan Ivanov for the experimental support and Milena Perovic and Heather Cavers for the fruitful discussions.

ORCID

Fabienne Huttner https://orcid.org/0000-0001-9244-6648

References

1. J. Baars, T. Domenech, R. Bleischwitz, H. E. Melin, and O. Heidrich, Oliver, "Circular economy strategies for electric vehicle batteries reduce reliance on raw materials." *Nat. Sustain.*, **4**, 71 (2021).
2. Z. P. Cano, D. Banham, S. Ye, A. Hintennach, J. Lu, M. Fowler, and Z. Chen, "Batteries and fuel cells for emerging electric vehicle markets." *Nat. Energy*, **3**, 279 (2018).
3. X. Fan, G. Hu, B. Zhang, X. Ou, J. Zhang, W. Zhao, H. Jia, L. Zou, P. Li, and Y. Yang, "Crack-free single-crystalline Ni-rich layered NCM cathode enable superior cycling performance of lithium-ion batteries." *Nano Energy*, **70**, 104450 (2020).
4. H. Zheng, G. Liu, X. Song, P. Ridgway, S. Xun, and V. S. Battaglia, "Cathode performance as a function of inactive material and void fractions." *J. Electrochem. Soc.*, **157**, A1060 (2010).
5. F. Huttner, W. Haselrieder, and A. Kwade, "The influence of different post-drying procedures on remaining water content and physical and electrochemical properties of lithium-ion batteries." *Energy Technol.*, **8**, 1900245 (2019).
6. A. Kwade, W. Haselrieder, R. Leithoff, A. Modlinger, F. Dietrich, and K. Droeder, "Current status and challenges for automotive battery production technologies." *Nat. Energy*, **3**, 290 (2018).
7. H. Dreger, W. Haselrieder, and A. Kwade, "Influence of dispersing by extrusion and calendering on the performance of lithium-ion battery electrodes." *J. Energy Storage*, **21**, 231 (2019).
8. F. Huttner, A. Marth, J. C. Eser, T. Heckmann, J. Mohacsi, J. K. Mayer, P. Scharfer, W. Schabel, and A. Kwade, "Design of vacuum post-drying procedures for electrodes of lithium-ion batteries." *Batteries Supercaps*, **4**, 1499 (2021).
9. M. Stich, N. Pandey, and A. Bund, "Drying and moisture resorption behaviour of various electrode materials and separators for lithium-ion batteries." *J. Power Sources*, **364**, 84 (2017).
10. U. Langklotz, M. Schneider, and A. Michaelis, "Water uptake of tape-cast cathodes for lithium ion batteries." *J. Ceram. Sci. Technol.*, **04**, 69 (2013).
11. J. Vetter, P. Novák, M. R. Wagner, C. Veit, K.-C. Möller, J. O. Besenhard, M. Winter, M. Wohlfahrt-Mehrens, C. Vogler, and A. Hammouche, "Ageing mechanisms in lithium-ion batteries." *J. Power Sources*, **147**, 269 (2005).
12. S. Nowak and M. Winter, "Elemental analysis of lithium ion batteries." *J. Anal. At. Spectrom.*, **32**, 1833 (2017).
13. D. Yang, X. Li, N. Wu, and W. Tian, "Effect of moisture content on the electrochemical performance of $LiNi_{1/3}Co_{1/3}Mn_{1/3}O_2$/graphite battery." *Electrochim. Acta*, **188**, 611 (2016).
14. J. C. Eser, T. Wirsching, P. G. Weidler, A. Altvater, T. Börnhorst, J. Kumberg, G. Schöne, M. Müller, P. Scharfer, and W. Schabel, "Moisture adsorption behavior in anodes for Li-ion batteries." *Energy Technol.*, **8**, 1801162 (2020).
15. C. Meyer, M. Kosfeld, W. Haselrieder, and A. Kwade, "Process modeling of the electrode calendering of lithium-ion batteries regarding variation of cathode active materials and mass loadings." *J. Energy Storage*, **18**, 371 (2018).
16. W. Haselrieder, S. Ivanov, D. K. Christen, H. Bockholt, and A. Kwade, "Impact of the calendering process on the interfacial structure and the related electrochemical performance of secondary lithium-ion batteries." *ECS Trans.*, **50**, 59 (2013).
17. H. Zheng, L. Tan, G. Liu, X. Song, and V. S. Battaglia, "Calendering effects on the physical and electrochemical properties of Li[Ni1/3Mn1/3Co1/3]O_2 cathode." *J. Power Sources*, **208**, 52 (2012).
18. D. Schmidt, M. Kamlah, and V. Knoblauch, "Highly densified NCM-cathodes for high energy Li-ion batteries: microstructural evolution during densification and its influence on the performance of the electrodes." *J. Energy Storage*, **17**, 213 (2018).
19. W. A. Appiah, J. Park, S. Song, S. Byun, M.-H. Ryou, and Y. M. Lee, "Design optimization of $LiNi_{0.6}Co_{0.2}Mn_{0.2}O_2$/graphite lithium-ion cells based on simulation and experimental data." *J. Power Sources*, **319**, 147 (2016).
20. C. Meyer, M. Weyhe, W. Haselrieder, and A. Kwade, "Heated calendering of cathodes for lithium-ion batteries with varied carbon black and binder contents." *Energy Technol.*, **8**, 1900175 (2020).
21. C. Meyer, H. Bockholt, W. Haselrieder, and A. Kwade, "Characterization of the calendering process for compaction of electrodes for lithium-ion batteries." *J. Mater. Process. Technol.*, **249**, 172 (2017).
22. S. Oswald, D. Pritzl, M. Wetjen, and H. A. Gasteiger, "Novel method for monitoring the electrochemical capacitance by *in situ* impedance spectroscopy as indicator for particle cracking of nickel-rich NCMs: part i. theory and validation." *J. Electrochem. Soc.*, **167**, 100511 (2020).
23. W. Haselrieder, *Kalandrierung zur Gezielten Einstellung der Batterieelektroden-Performance (Thesis)*, Technische Universität Braunschweig; Internationaler Fachverlag für Wissenschaft & Praxis, Göttingen (2016).
24. J. Choi, B. Son, M.-H. Ryou, S. H. Kim, J. M. Ko, and Y. M. Lee, "Effect of $LiCoO_2$ cathode density and thickness on electrochemical performance of lithium-ion batteries." *J. Electrochem. Sci. Technol.*, **4**, 27 (2013).
25. T. Günther, D. Schreiner, A. Metkar, C. Meyer, A. Kwade, and G. Reinhart, "Classification of calendering-induced electrode defects and their influence on subsequent processes of lithium-ion battery production." *Energy Technol.*, **8**, 1900026 (2020).
26. C. Schilcher, C. Meyer, and A. Kwade, "Structural and electrochemical properties of calendered lithium manganese oxide cathodes." *Energy Technol.*, **4**, 1604 (2016).
27. H. Y. Tran, G. Greco, C. Täubert, M. Wohlfahrt-Mehrens, W. Haselrieder, and A. Kwade, "Influence of electrode preparation on the electrochemical performance of $LiNi_{0.8}Co_{0.15}Al_{0.05}O_2$ composite electrodes for lithium-ion batteries." *J. Power Sources*, **210**, 276 (2012).
28. M. Indrikova, S. Grundwald, F. Golks, A. Netz, B. Westphal, and A. Kwade, "The morphology of battery electrodes with the focus of the conductive additives paths." *J. Electrochem. Soc.*, **162**, A2021 (2015).
29. Z. An, Y. Li, R. Xu, F. Dai, Y. Zhao, and L. Chen, "New insights in poly(vinylidene fluoride) (PVDF) membrane hemocompatibility: synergistic effect of PVDF-g-(acryloyl morpholine) and PVDF-g-(poly(acrylic acid)-argatroban) copolymers." *Appl. Surf. Sci.*, **457**, 170 (2018).
30. A. Grosman and C. Ortega, "Capillary condensation in porous materials. hysteresis and interaction mechanism without pore blocking/percolation process." *Langmuir*, **24**, 3977 (2008).
31. L. O. Figura, *Lebensmittelphysik-Physikalische Kenngrößen - Messung und Anwendung* (Springer, Berlin Heidelberg) (2004).
32. M. Krus, *Feuchtetransport- und Speicherkapazitäten poröser mineralischer Baustoffe. Teoretische Grundlagen und neue Meßtechniken (Thesis)*, Universität Stuttgart, Stuttgart (1995).
33. O. Claussen, *Elasticity and Morphology of Wet Fiber Networks (Thesis)*, Georg-August-Universität Göttingen, Göttingen (2011).
34. J. Sicklinger, M. Metzger, H. Beyer, D. Pritzl, and H. Gasteiger, "Ambient storage derived surface contamination of NCM811 and NCM111: performance implications and mitigation strategies." *J. Electrochem. Soc.*, A2322 (2019).
35. J. C. Eser, B. Deichmann, T. Wirsching, P. G. Weidler, P. Scharfer, and W. Schabel, "Hysteresis behavior in the sorption equilibrium of water in anodes for Li-Ion batteries." *Langmuir*, **36**, 6193 (2020).
36. W. Schabel, I. Mamaliga, and M. Kind, "Messungen von sorptionsisothermen *u*nd diffusionskoeffizienten in polymerlösungen." *Chem. Ing. Tech.*, **75**, 36 (2003).
37. S. Brunauer, P. H. Emmett, and E. Teller, "Adsorption of gases in multimolecular layers." *J. Am. Chem. Soc.*, **60**, 309 (1938).
38. I. Langmuir, "The adsorption of gases on plane surfaces of glass, mica and platinum." *J. Am. Chem. Soc.*, **40**, 1361 (1918).
39. W. Haselrieder, B. Westphal, H. Bockholt, A. Diener, S. Höft, and A. Kwade, "Measuring the coating adhesion strength of electrodes for lithium-ion batteries." *Int. J. Adhes. Adhes.*, **60**, 1 (2015).
40. B. G. Westphal, N. Mainusch, C. Meyer, W. Haselrieder, M. Indrikova, P. Titscher, H. Bockholt, W. Viöl, and A. Kwade, "Influence of high intensive dry mixing and calendering on relative electrode resistivity determined via an advanced two point approach." *J. Energy Storage*, **11**, 76 (2017).
41. L. Froboese, P. Titscher, B. Westphal, W. Haselrieder, and A. Kwade, "Mercury intrusion for ion- and conversion-based battery electrodes—structure and diffusion coefficient determination." *Mater. Charact.*, **133**, 102 (2017).
42. M. Ebner, F. Geldmacher, F. Marone, M. Stampanoni, and V. Wood, "X-ray tomography of porous, transition metal oxide based lithium ion battery electrodes." *Adv. Energy Mater.*, **3**, 845 (2013).

43. L. R. Fisher, R. A. Gamble, and J. Middlehurst, "The Kelvin equation and the capillary condensation of water." *Nature*, **290**, 575 (1981).
44. L. R. Fisher and J. N. Israelachvili, "Direct experimental verification of the Kelvin equation for capillary condensation." *Nature*, **277**, 548 (1978).
45. B. Li, *Capillary pressure in nanopores: deviation from young-laplace equation (Thesis)*, Texas A&M University, Texas (2017).
46. D. R. Sandoval, W. Yan, M. L. Michelsen, and E. H. Stenby, "The phase envelope of multicomponent mixtures in the presence of a capillary pressure difference." *Ind. Eng. Chem. Res.*, **55**, 6530 (2016).
47. H. Chen, M. Ling, L. Hencz, H. Y. Ling, G. Li, Z. Lin, G. Liu, and S. Zhang, "Exploring chemical, mechanical, and electrical functionalities of binders for advanced energy-storage devices." *Chem. Rev.*, **118**, 8936 (2018).
48. F. P. Bowden and J. E. Young, "Friction of diamond, graphite, and carbon and the influence of surface films." *Royal Society*, **208**, A212 (1951).
49. C. Sangrós Giménez, C. Schilde, L. Froböse, S. Ivanov, and A. Kwade, "Mechanical, electrical, and ionic behavior of lithium-ion battery electrodes via discrete element method simulations." *Energy Technol.*, **8**, 1900180 (2020).
50. C. Heubner, A. Nickol, J. Seeba, S. Reuber, N. Junker, M. Wolter, M. Schneider, and A. Michaelis, "Understanding thickness and porosity effects on the electrochemical performance of $LiNi_{0.6}Co_{0.2}Mn_{0.2}O_2$-based cathodes for high energy Li-ion batteries." *J. Power Sources*, **419**, 119 (2019).
51. C. Heubner, M. Schneider, and A. Michaelis, "Diffusion-limited C-rate: a fundamental principle quantifying the intrinsic limits of li-ion batteries." *Adv. Energy Mater.*, **10**, 1902523 (2020).
52. R. Ruess, S. Schweidler, H. Hemmelmann, G. Conforto, A. Bielefeld, D. A. Weber, J. Sann, M. T. Elm, and J. Janek, "Influence of NCM particle cracking on kinetics of lithium-ion batteries with liquid or solid electrolyte." *J. Electrochem. Soc.*, **167**, 100532 (2020).
53. E. Trevisanello, R. Ruess, G. Conforto, F. H. Richter, and J. Janek, "Polycrystalline and single crystalline NCM Cathode materials—quantifying particle cracking, active surface area, and lithium diffusion." *Adv. Energy Mater.*, **11**, 2003400 (2021).
54. G. Inoue and M. Kawase, "Numerical and experimental evaluation of the relationship between porous electrode structure and effective conductivity of ions and electrons in lithium-ion batteries." *J. Power Sources*, **342**, 476 (2017).
55. R. Dominko, M. Gaberscek, J. Drofenik, M. Bele, S. Pejovnik, and J. Jamnik, "The role of carbon black distribution in cathodes for Li ion batteries." *J. Power Sources*, **119–121**, 770 (2003).